Applied Energy 228 (2018) 279–288

Contents lists available at ScienceDirect

Applied Energy

journal homepage: www.elsevier.com/locate/apenergy

Networked microgrid stability through distributed formal analysis

Yan Li[a], Peng Zhang[a,*], Meng Yue[b]

[a] Department of Electrical and Computer Engineering, University of Connecticut, Storrs, CT 06269, USA
[b] Sustainable Energy Technologies Department, Brookhaven National Laboratory, Upton, NY 11973, USA

HIGHLIGHTS

- A scalable distributed formal analysis (DFA) is devised for stability analysis of networked microgrids under disturbances.
- A distributed quasi-diagonalized Geršgorin (DQG) theory is developed to identify systems' stability margins.
- A microgrid-oriented decomposition approach is established to decouple networked microgrids.
- A novel framework is designed to effectively implement DQG-based DFA in networked microgrids.

ARTICLE INFO

Keywords:
Networked microgrids
Stability
Distributed formal analysis (DFA)
Distributed quasi-diagonalized Geršgorin (DQG) theory
Reachable set

ABSTRACT

A scalable distributed formal analysis (DFA) via reachable set computation is presented to efficiently evaluate the stability of networked microgrids under disturbances induced by distributed energy resources (DERs). With mathematical rigor, DFA can efficiently compute the boundaries of all possible dynamics in a distributed way, which are unattainable via traditional time-domain simulations or direct methods. A distributed quasi-diagonalized Geršgorin (DQG) theory is then combined with DFA to identify systems' stability margins. A microgrid-oriented decomposition approach is established to decouple a networked microgrid system and enable calculations of DFA and DQG while also preserving the privacy of each subsystem. Numerical tests on a networked microgrid system validate that DFA and DQG facilitate the efficient calculation and analysis of networked microgrids' stability.

1. Introduction

Networked microgrids are a cluster of microgrids interconnected in close electrical or spatial proximity with coordinated energy management [1–3] and interactive supports between each other [4–6]. They have demonstrated flexibility in accommodating distributed energy resources (DERs) [7,8] and resiliency benefits to electricity customers [9,10]. However, the low inertia nature of DERs' power-electronics interfaces makes networked microgrids highly sensitive to disturbances or even leads to stability issues [11,12]. These disturbances could be intermittent generations from photovoltaics (PV) or wind [13], and episodic loads produced by the plugin of hybrid electric vehicles [14]. The challenge here is that it can be prohibitively expensive to directly evaluate these disturbances' impacts DERs or loads can have on the dynamics of a large-scale network microgrid system.

One intractable problem is the difficulty of using existing methods to tackle the stability issues arising from the near-infinite number of scenarios caused by DER integration [15]. There exist two major categories of stability assessment methods: time domain [16,17] or frequency domain simulation approaches [18] and direct methods [19]. The former approaches can compute operation trajectories based on a specified system structure and initial condition, but they have limited capability in handling parametric or input uncertainties [20]. Direct methods are able to identify regions of attraction, but they need to construct appropriate Lyapunov functions [19,21] or contraction functions [22], which is difficult or even impossible in reality.

Moreover, centralized stability calculation and evaluation may be impractical for dealing with a large-scale networked microgrid system due to calculation burden or privacy issue [23,24]. Many system decomposition techniques offer potential ways to tackle this problem. A hierarchical spectral clustering methodology was adopted in [25] to reveal the internal connectivity structure of a power transmission system, in order to properly partition a large-scale system. However, the eigenvalues and eigenvectors of a matrix correlated to the network are needed to calculate, which significantly increases computational burden and highly limits the application of this method. A multi-area Thévenin equivalent circuit approach was used in [26], which more focuses on optimally dividing the computation among PC cluster

* Corresponding author.
E-mail address: peng.zhang@uconn.edu (P. Zhang).

https://doi.org/10.1016/j.apenergy.2018.06.038
Received 13 April 2018; Received in revised form 31 May 2018; Accepted 7 June 2018
Available online 24 June 2018

processors. A waveform relaxation method was used in [27] for transient stability simulations, where subsystems' information are still shared between them. Therefore, how to effectively decouple a large-scale networked system and evaluate its stability is still an open problem.

In order to overcome the limitations of existing technologies, a scalable distributed formal analysis (DFA) approach and a distributed quasi-diagonalized Geršgorin (DQG) theory are presented to efficiently investigate the stability of networked microgrids under disturbances. The novelties of DFA and DQG are threefold:

(1) DFA can efficiently obtain the possible operation ranges of a networked microgrid system under disturbances, rather than repeatedly simulating and analyzing the system with on-going disturbances.
(2) DFA and DQG are fully distributed approaches with only limited amount of information exchanged between neighboring systems. Therefore, not only can they make a full use of distributed computing resources, but also potentially prevent the privacy leakage problem.
(3) DQG-enabled DFA is able to estimate the stability margin of a networked microgrid system under uncertain conditions.

The remainder of this paper is organized as follows: Section 2 and Section 3 establish the methodological foundations of DFA and DQG, respectively. Section 4 describes partitioning a large-scale networked microgrid system via microgrid-oriented decomposition method, and disturbances modeling via zonotope technique. Section 5 discusses the implementation of DFA and DQG. The feasibility and effectiveness of DFA and DQG have been validated through tests on a typical networked microgrid in Section 6. Conclusions are drawn in Section 7.

2. Distributed formal analysis via reachable set

DFA aims at finding the bounds of all possible system trajectories under various disturbances. Mathematically, the aim is to find reachable sets which can cover all possible dynamics [28,29].

2.1. Distributed formal analysis

Assuming that a large-scale system can be partitioned into several subsystems of lower dimensions, the reachable sets of the overall interconnected system can be obtained based on the formal analysis results from each subsystem as shown in (1) and (2) [30,31].

$$\mathscr{R}_s^e(t_{k+1}) = \varphi_1\mathscr{R}_1^e(t_{k+1}) \times \varphi_2\mathscr{R}_2^e(t_{k+1}) \times \cdots \times \varphi_n\mathscr{R}_n^e(t_{k+1}), \tag{1}$$

$$\mathscr{R}_s^e(\tau_k) = \varphi_1\mathscr{R}_1^e(\tau_k) \times \varphi_2\mathscr{R}_2^e(\tau_k) \times \cdots \times \varphi_n\mathscr{R}_n^e(\tau_k), \tag{2}$$

where $\mathscr{R}_s^e(t_{k+1})$ is the reachable set of the overall system at each time step, $\mathscr{R}_s^e(\tau_k)$ is the reachable set of the overall system during time steps, n is the number of subsystems, which is discussed in Section 4, $\times$ is Cartesian product [32], $\mathscr{R}_i^e(t_{k+1})$ is the reachable set of the ith subsystem at each time step, $\mathscr{R}_i^e(\tau_k)$ is the reachable set of the ith subsystem between time steps, and φ_i is a matrix, which contain ones when states are correlated and zeros otherwise an thus projects the local states of the ith subsystem to the states of the overall system.

2.2. Formal analysis in each subsystem

The reachable sets, $\mathscr{R}_i^e(t_{k+1})$ and $\mathscr{R}_i^e(\tau_k)$, in the ith subsystem can be calculated through the following two steps.

2.2.1. Dynamics abstraction of subsystems

If the ith dynamic subsystem can be expressed by a set of nonlinear differential-algebraic equations (DAEs) [33], the dynamics of this subsystem can be analyzed by abstracting the original DAEs into linear differential inclusions at each time step, which is discussed in detail in Section 4. Then the reachability model of the ith subsystem under uncertainties can be expressed as follows:

$$\Delta\dot{\mathbf{x}}_\mathbf{i} \in \mathbf{A_i}\Delta\mathbf{x_i} \oplus \mathbf{P_i}, \tag{3}$$

where $\Delta\mathbf{x_i} = \mathbf{x_i} - \mathbf{x_{i,0}}$, $\mathbf{x_{i,0}}$ is the operation point where the subsystem is linearized, $\mathbf{A_i} = [a_{jk}] \in \mathbb{R}^{m\times m}$ is the state matrix, m is the dimension of the ith subsystem, $\oplus$ is Minkowski addition [28], and $\mathbf{P_i}$ is a set of uncertain inputs which can be either formulated using a point-based approach or a set-based one as is adopted in this paper and discussed in Section 4 [28].

2.2.2. Reachable set computation in each subsystem

The reachable set of the ith subsystem can be obtained at each simulation time step via a closed-form solution as follows [28,30,34]:

$$\mathscr{R}_i^e(t_{k+1}) = \phi(\mathbf{A_i}, r)\mathscr{R}_i^e(t_k) \oplus \Psi(\mathbf{A_i}, r, \mathbf{p_{i,0}}) \oplus I_p^e(\mathbf{p_{i,\Delta}}, r), \tag{4}$$

$$\mathscr{R}_i^e(\tau_k) = C(\mathscr{R}_i^e(t_k), \phi(\mathbf{A_i}, r)\mathscr{R}_i^e(t_k) \oplus \Psi(\mathbf{A_i}, r, \mathbf{p_{i,0}})) \oplus I_p^e(\mathbf{p_{i,\Delta}}, r) \oplus I_\xi^e, \tag{5}$$

where $r = t_{k+1} - t_k$ is the time interval, $C(\cdot)$ represents convex hull calculation, and $\phi(\mathbf{A_i}, r)$ represents how the history reachable set $\mathscr{R}_i^e(t_k)$ in the ith subsystem contributes to the current reachable set $\mathscr{R}_i^e(t_{k+1})$, with its expression given as follows:

$$\phi(\mathbf{A_i}, r) = e^{\mathbf{A}r}, \tag{6}$$

where $e^{\mathbf{A}r}$ is calculated by integrating the finite Taylor series $\sum_{j=0}^{\eta} \frac{(\mathbf{A_i}r)^j}{j!}$ up to order η [30]. The increment of reachable set caused by deterministic inputs $\mathbf{p_{i,0}}$ and uncertain ones $\mathbf{p_{i,\Delta}}$ are represented by $\Psi(\mathbf{A_i}, r, \mathbf{p_{i,0}})$ and $I_p^e(\mathbf{p_{i,\Delta}}, r)$, respectively:

$$\Psi(\mathbf{A_i}, r, \mathbf{p_{i,0}}) = \left\{ \sum_{j=0}^{\eta} \frac{\mathbf{A_i}^j r^{j+1}}{(j+1)!} \oplus [-X(\mathbf{A_i}, r)r, X(\mathbf{A_i}, r)r] \right\} \mathbf{p_{i,0}}, \tag{7}$$

$$I_p^e(\mathbf{p_{i,\Delta}}, r) = \sum_{j=0}^{\eta} \left(\frac{\mathbf{A_i}^j r^{j+1}}{(j+1)!} \mathbf{p_{i,\Delta}} \right) \oplus \{[-X(\mathbf{A_i}, r)r, X(\mathbf{A_i}, r)r] \cdot \mathbf{p_{i,\Delta}}\}. \tag{8}$$

I_ξ^e denotes the increment in reachable set caused by curvature of trajectories from t_k to t_{k+1}.

$$I_\xi^e = \{(I \oplus [-X(\mathbf{A_i}, r), X(\mathbf{A_i}, r)]) \cdot \mathscr{R}_i^e(t_k)\} \oplus \{(\widetilde{I} \oplus [-X(\mathbf{A_i}, r)r, X(\mathbf{A_i}, r)r]) \cdot \mathbf{p_{i,0}}\}, \tag{9}$$

where $X(\mathbf{A_i}, r)$, I, $\widetilde{I}$ involved in 7–9 are given as follows:

$$X(\mathbf{A_i}, r) = e^{|\mathbf{A_i}|r} - \sum_{j=0}^{\eta} \frac{(|\mathbf{A_i}|r)^j}{j!}, \tag{10}$$

$$I = \sum_{j=2}^{\eta} \left[(j^{\frac{-j}{j-1}} - j^{\frac{-1}{j-1}}) r^j, 0 \right] \frac{\mathbf{A_i^j}}{j!}, \tag{11}$$

$$\widetilde{I} = \sum_{j=2}^{\eta+1} \left[(j^{\frac{-j}{j-1}} - j^{\frac{-1}{j-1}}) r^j, 0 \right] \frac{\mathbf{A_i}^{j-1}}{j!}. \tag{12}$$

3. Distributed quasi-diagonalized Geršgorin theory

Geršgorin Theorem is a powerful method for efficiently estimating eigenvalues of a dynamical system under disturbances. An enhanced distributed quasi-diagonalized Geršgorin theory is established in this section and used to evaluate the stability margin in Section 5.

3.1. Geršgorin sets estimation

Assuming that $\mathbf{A_i}$ is the state matrix of the ith dynamic subsystem, one can describe the eigenvalue problem which reflects the small signal

stability of the subsystem as follows [12]:

$$\mathbf{A_i v_j} = \lambda_j \mathbf{v_j}, \tag{13}$$

$$\mathbf{A_i^T u_j} = \lambda_j \mathbf{u_j}. \tag{14}$$

where λ_j is the jth generalized eigenvalue of the ith subsystem, $\mathbf{v_j}$ and $\mathbf{u_j^T}$ are the jth right and left eigenvector, respectively, satisfying the orthogonal normalization conditions as shown in (15) [33].

$$\mathbf{u_j^T v_k} = \delta_{jk}, \tag{15}$$

$$\mathbf{u_j^T A_i v_k} = \delta_{jk}\lambda_j, \tag{16}$$

where δ_{jk} is the Kronecker sign.

Instead of calculating the exact eigenvalues λ_j, the eigenvalue range can be estimated directly based on the state matrix $\mathbf{A_i}$ by using the Geršgorin disk and set obtained via the following Geršgorin Theorem.

Theorem 1. *For any non-singular finite-dimensional matrix $\mathbf{A_i}$ with λ_j as its jth eigenvalue, there is a positive integer k in $L=1,2,\ldots,l$ such that,*

$$|\lambda_j - a_{kk}| \leqslant r_k(\mathbf{A_i}), \tag{17}$$

where $r_k(\mathbf{A_i}) \doteq \sum_{s\in L\setminus\{k\}} |a_{ks}|$. If $\sigma(\mathbf{A_i})$ denotes a set of all eigenvalues of $\mathbf{A_i}$, then $\sigma(\mathbf{A_i})$ satisfies the following condition:

$$\sigma(\mathbf{A_i}) \subseteq \Gamma(\mathbf{A_i}) \doteq \cup_{k=1}^{l} \Gamma_k(\mathbf{A_i}), \tag{18}$$

where $\Gamma(\mathbf{A_i})$ is the Geršgorin set of non-singular matrix $\mathbf{A_i}$, $\Gamma_k(\mathbf{A_i})$ is the kth Geršgorin disk, and can be expressed as $\Gamma_k(\mathbf{A_i}) \doteq \{|x - a_{kk}| \leqslant r_k(\mathbf{A_i}), x \in \mathbb{R}\}$.

3.2. Distributed quasi-diagonalized Geršgorin sets estimation

From (17), it can be seen that the eigenvalue distributions are usually over-approximated when the state matrix $\mathbf{A_i}$ is not strongly diagonally dominant. Therefore, diagonalizing the state matrix is critical to reduce the conservativeness of the conventional Geršgorin theory and to improve the estimation accuracy of eigenvalue distributions. Taking into account the orthogonal normalization conditions shown in (16), the state matrix $\mathbf{A_i}$ under system disturbances can be quasi-diagonalized as follows:

$$\mathbf{U_{i,0}^T A_i V_{i,0}} = \mathbf{U_{i,0}^T A_{i,0} V_{i,0}} + \mathbf{U_{i,0}^T A_{i,P} V_{i,0}} = \mathbf{S_{i,0}} + \mathbf{S_{i,P}}, \tag{19}$$

where $\mathbf{A_{i,0}}$ is the state matrix of the ith subsystem at the operation point $\mathbf{x_{i,0}}$, $\mathbf{S_{i,0}}$, $\mathbf{U_{i,0}^T}$ and $\mathbf{V_{i,0}}$ are the corresponding eigenvalue matrix, left eigenvector matrix, and right eigenvector matrix at $\mathbf{x_{i,0}}$, respectively, $\mathbf{A_{i,P}}$ is the increment of state matrix under disturbances, which is constructed via a set-based technique and analyzed in Section 4, and $\mathbf{S_{i,P}}$ is the corresponding increment of eigenvalue matrix. Thus, the eigenvalue problem of a system under disturbances is transformed to the analysis of the matrix $\mathbf{S_{i,P}}$. According to Theorem 1, the following expressions can be obtained in each subsystem.

$$\Gamma_k(\mathbf{S_{Si,P}}) = \{|x - s_{kk}| \leqslant r_k(\mathbf{S_{Si,P}}), x \in \mathbb{R}\}, \tag{20}$$

$$\sigma_k(\mathbf{S_{i,P}}) \subseteq \Gamma(\mathbf{S_{i,P}}) \doteq \cup_{k=1}^{n} \Gamma_k(\mathbf{S_{i,P}}). \tag{21}$$

Therefore, the distribution of the kth eigenvalue in the ith subsystem under uncertainties can be expressed as a Geršgorin disk with $\mathbf{S_{i,0}}$ as its center and $\Gamma_k(\mathbf{S_{i,P}})$ as its corresponding area.

3.3. Quasi-diagonalized Geršgorin sets estimation in the overall system

After Geršgorin sets correlated to each subsystem are calculated, the following equations are used to obtain the Geršgorin results in the overall system.

$$\Gamma(\mathbf{S_P}) = \varphi_1\Gamma(\mathbf{S_{1,P}}) \times \varphi_2\Gamma(\mathbf{S_{2,P}}) \times \cdots \times \varphi_n\Gamma(\mathbf{S_{n,P}}), \tag{22}$$

$$\sigma(\mathbf{S_P}) = \varphi_1\sigma(\mathbf{S_{1,P}}) \times \varphi_2\sigma(\mathbf{S_{2,P}}) \times \cdots \times \varphi_n\sigma(\mathbf{S_{n,P}}), \tag{23}$$

where $\Gamma(\mathbf{S_P})$ and $\sigma(\mathbf{S_P})$ are the Geršgorin disk and sets of the overall system, $\Gamma(\mathbf{S_{i,P}})$ and $\sigma(\mathbf{S_{i,P}})$ are the Geršgorin disk and sets of the ith subsystem, $\times$ is Cartesian product and φ_i is the mapping matrix which is the same with that in (1) and (2).

4. DFA and DQG in networked microgrids

A microgrid-oriented decomposition approach is presented in this section, based on which DFA and DQG are implemented. Meanwhile, a zonotope technique is introduced to model set-based disturbances instead of using a point-based one [34].

4.1. Microgrid-oriented decomposition

When power-electronic interfaces of DERs are modeled using dynamic averaging method [33], a set of DAEs shown in (24) and (25) is usually adopted to model a networked microgrid integrated with DERs.

$$\dot{\mathbf{x}} = \mathbf{F}(\mathbf{x}, \mathbf{y}, \mathbf{p}), \tag{24}$$

$$\mathbf{0} = \mathbf{G}(\mathbf{x}, \mathbf{y}, \mathbf{p}), \tag{25}$$

where $\mathbf{x} \in \mathbb{R}^x$ is the state variable vector (e.g., integral variable in DER controllers), $\mathbf{y} \in \mathbb{R}^y$ is the algebraic variable vector (e.g., bus voltage), and $\mathbf{p} \in \mathbb{R}^p$ is the disturbance vector. Obviously, microgrids are coupled together via the algebraic equations in (25) as shown in Fig. 1(a). Therefore, the key point of partitioning a large-scale networked microgrid is to decouple the algebraic equations. Taking into account the feasibility of partitioning and calculation burden, a microgrid-oriented decomposition is adopted here as shown in Fig. 1(b). By introducing an interface vector $\mathbf{S_{i,j}}$, the original networked system can be decoupled into several individual subsystems. The algebraic equation set in (25) are then separated into multiple sets correspondingly, as given in (26).

$$\mathbf{Y_i \cdot V_i \circ \overline{V}_i} + \mathbf{S_{G,i} - S_{L,i} - S_{i,j}} = \mathbf{0}, \tag{26}$$

where $\circ$ is the Hadamard product [35], $\mathbf{Y_i}$ is the modified admittance matrix of the ith subsystem under system partition [28], $\mathbf{V_i}$ is the corresponding bus voltage vector [28], $\mathbf{\overline{V}_i}$ is the extended bus voltage vector $[\mathbf{V_i}, \mathbf{V_i}]$, $\mathbf{S_{G,i}}$ is the power injection vector, $\mathbf{S_{L,i}}$ is the power load vector, $\mathbf{S_{i,j}}$ is the exchange power on the interface of the ith subsystem with its neighbors.

The advantages of the microgrid-oriented decomposition technique include:

- The matrices of admittance, voltage, and power are formulated in modules, which enables 'plug and play' and flexible decompositions.
- Only interface data are exchanged between neighbors, which helps ensure data security [36]. In the future, a privacy-preserving technique [37] will be used to ensure the integrity and confidentiality of the interface data, and to protect against attacks.

Based on the aforementioned system decomposition, the ith subsystem can be linearized at the operation point $\mathbf{x_{i,0}}$. When the high-order Taylor expansion is neglected, the following equations can be obtained [28].

$$\dot{\mathbf{x}}_\mathbf{i} = \mathbf{f_i}(\mathbf{x_{i,0}}, \mathbf{y_{i,0}}, \mathbf{p_{i,0}}) + \frac{\partial \mathbf{f_i}}{\partial \mathbf{x_i}}\Delta\mathbf{x_i} + \frac{\partial \mathbf{f_i}}{\partial \mathbf{y_i}}\Delta\mathbf{y_i} + \frac{\partial \mathbf{f_i}}{\partial \mathbf{p_i}}\Delta\mathbf{p_i} \tag{27}$$

$$\mathbf{0} = \mathbf{g_i}(\mathbf{x_{i,0}}, \mathbf{y_{i,0}}, \mathbf{p_{i,0}}) + \frac{\partial \mathbf{g_i}}{\partial \mathbf{x_i}}\Delta\mathbf{x_i} + \frac{\partial \mathbf{g_i}}{\partial \mathbf{y_i}}\Delta\mathbf{y_i} + \frac{\partial \mathbf{g_i}}{\partial \mathbf{p_i}}\Delta\mathbf{p_i}, \tag{28}$$

where $\mathbf{f_i} \in \mathbf{F}$ represents the differential equations correlated to the ith subsystem, $\mathbf{g_i} \in \mathbf{G}$ represents the corresponding algebraic ones, i.e., (26), $\mathbf{f_{x_i}} = \partial\mathbf{f_i}/\partial\mathbf{x_i}$ is the partial derivative matrix of differential equations with respect to state variables, $\mathbf{f_{y_i}} = \partial\mathbf{f_i}/\partial\mathbf{y_i}$ is the partial derivative matrix of differential equations with respect to algebraic variables, $\mathbf{f_{p_i}} = \partial\mathbf{f_i}/\partial\mathbf{p_i}$ is the partial derivative matrix of differential equations

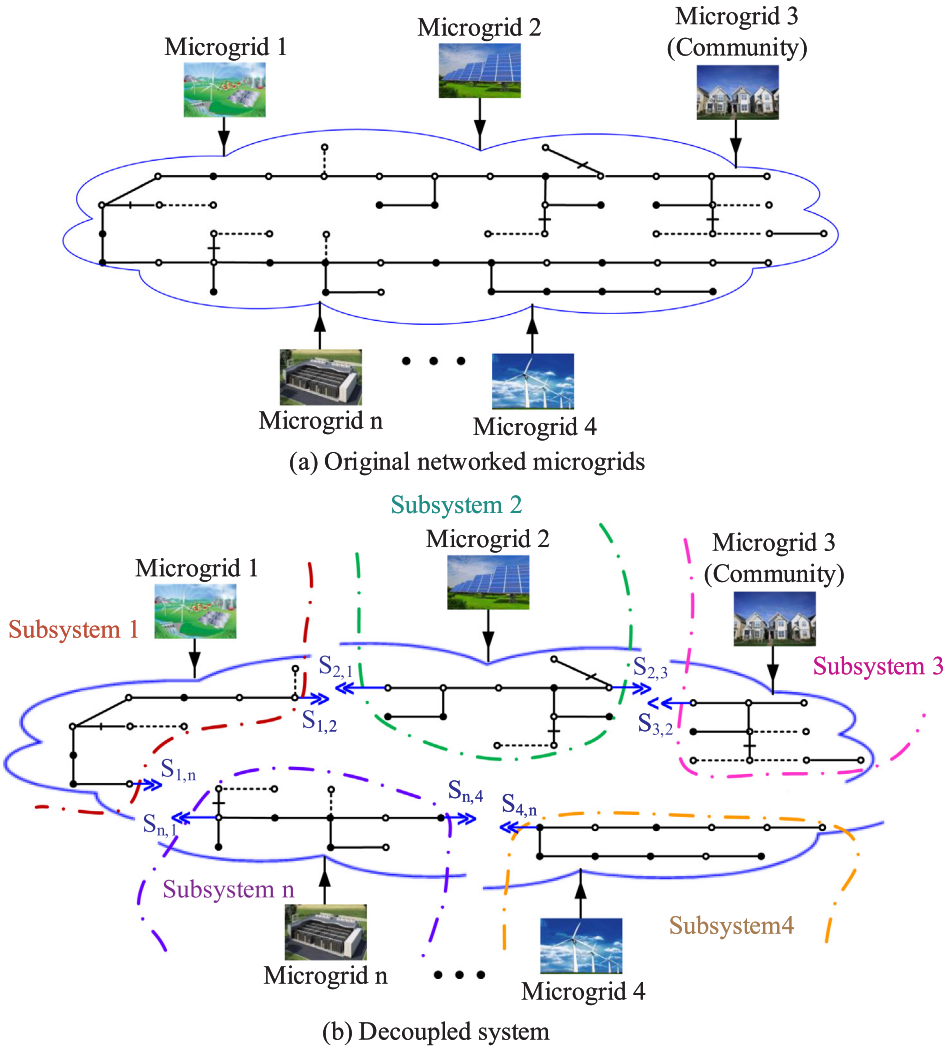

Fig. 1. Concept of microgrid-oriented partition.

with respect to disturbance variables, $\mathbf{g}_{\mathbf{x}_i} = \partial \mathbf{g}_i / \partial \mathbf{x}_i$ is the partial derivative matrix of algebraic equations with respect to state variables, $\mathbf{g}_{\mathbf{y}_i} = \partial \mathbf{g}_i / \partial \mathbf{y}_i$ is the partial derivative matrix of algebraic equations with respect to algebraic variables, and $\mathbf{g}_{\mathbf{p}_i} = \partial \mathbf{g}_i / \partial \mathbf{p}_i$ is the partial derivative matrix of algebraic equations with respect to disturbance variables. When $\mathbf{g}_{\mathbf{y}_i}$ is non-singular [38], the following equation can be obtained.

$$\Delta \dot{\mathbf{x}}_i = [\mathbf{f}_{\mathbf{x}_i} - \mathbf{f}_{\mathbf{y}_i} \mathbf{g}_{\mathbf{y}_i}^{-1} \mathbf{g}_{\mathbf{x}_i}] \Delta \mathbf{x}_i + [\mathbf{f}_{\mathbf{p}_i} - \mathbf{f}_{\mathbf{y}_i} \mathbf{g}_{\mathbf{y}_i}^{-1} \mathbf{g}_{\mathbf{p}_i}] \Delta \mathbf{p}_i. \tag{29}$$

Therefore, with linearization, the state matrix of the ith subsystem can be obtained at each time step.

$$\mathbf{A}_i = \mathbf{f}_{\mathbf{x}_i} - \mathbf{f}_{\mathbf{y}_i} \mathbf{g}_{\mathbf{y}_i}^{-1} \mathbf{g}_{\mathbf{x}_i}, \tag{30}$$

where $\mathbf{A}_i$ is equivalent to $\mathbf{A}_i$ in (3), (13), and (14), $[\mathbf{F}_\mathbf{p} - \mathbf{F}_\mathbf{y} \mathbf{G}_\mathbf{y}^{-1} \mathbf{G}_\mathbf{p}] \Delta \mathbf{p}$ is equivalent to $\mathbf{P}_i$ in (3).

4.2. Zonotope-based disturbances modeling

A proper model of disturbances is critical to formal analysis. Instead of using the traditional point-based methods, zonotope technique is adopted in this paper due to its high accuracy, good compactness of the representation, and low complexity [34,39].

A typical zonotope construction is shown in Fig. 2, based on which a zonotope $\mathscr{P}$ is usually modeled in (31).

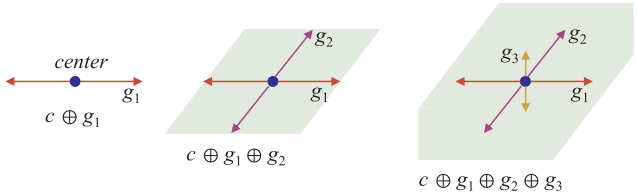

Fig. 2. Concept of zonotope.

$$\mathscr{P} = \left\{ \boldsymbol{c} + \sum_{i=1}^{m} \beta_i \mathbf{g}_i | \beta_i \in [-1, 1] \right\}, \tag{31}$$

where $c \in \mathbb{R}^n$ is the center of zonotope $\mathscr{P}$ and $g_i \in \mathbb{R}^n$ are its corresponding generators.

Therefore, by using (31), the uncertain input $\mathbf{P}_i$ in (3) can be expressed in a zonotope. For more accurate characterization of uncertainties, polynomial zonotopes and probabilistic zonotopes can be used.

5. Implementation of DQG-based DFA in networked microgrids

The DFA method integrated with DQG offers an option to effectively calculate and analyze the stability of a networked microgrid system under disturbances. The analysis procedure is illustrated in Fig. 3.

As shown in Fig. 3, an original interconnected microgrid system is

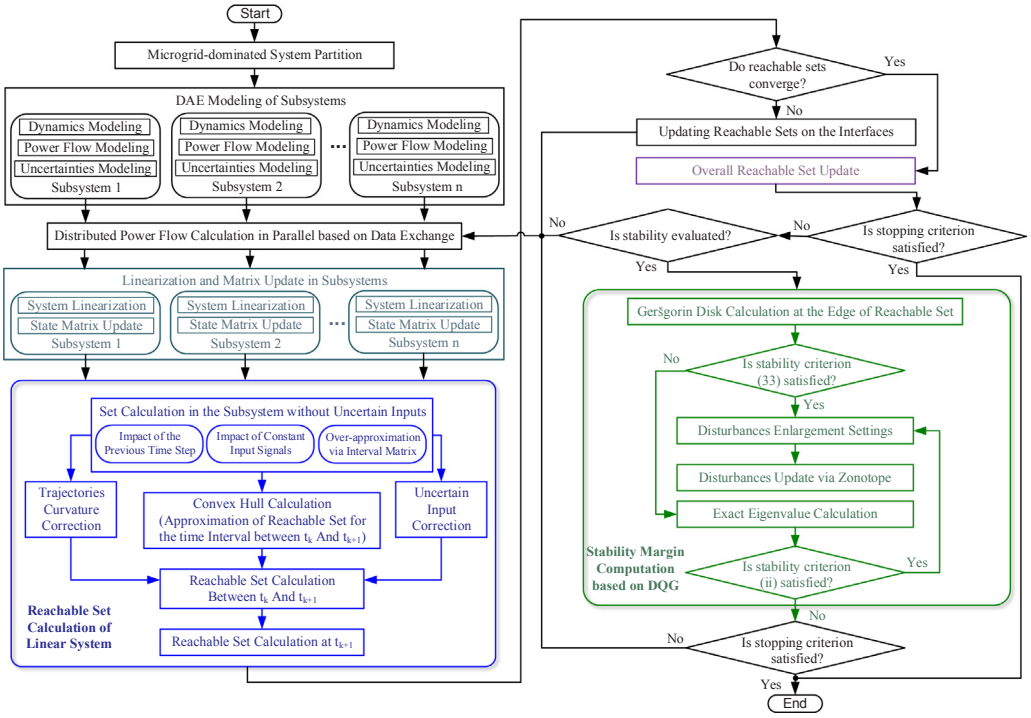

Fig. 3. Flowchart of DFA calculation.

partitioned into several subsystems based on the microgrid-oriented decomposition concept shown in Fig. 1. Then the dynamics, steady-state, and uncertainties involved in each subsystem are modeled using (24), (26), and (31), respectively. The steady-state, i.e., power flow, in each subsystem is then calculated in parallel based on data exchange between subsystems. An example is given in Section 6 to illustrate the iteration process of power flow computation. After power flows are solved in a distributed way, linearization can be conducted via (27) and (28) in each subsystems, based on which state matrix $\mathbf{A_i}$ can be obtained.

Then the DQG-based DFA can be implemented, which involves the following steps:

(1) DFA is used to computed the reachable sets of subsystems' states based on interface data exchanged between subsystems.
(2) DQG is sequentially used on the edges of reachable sets to calculate Geršgorin disks.
(3) Geršgorin disks are then evaluated to assess the stability condition of the overall system under disturbances.

5.1. Implementation of DFA

Reachable sets in each subsystem are calculated in parallel by using (4) and (5). More details about this calculation can be found in [28]. If the reachable sets of the subsystem interfaces converge, the overall reachable set can be obtained based on (1) and (2). Otherwise, the power flow will be updated and reachable sets in each subsystem will be computed in parallel again.

5.2. Implementation of DQG

When the reachable sets are obtained, DQG can be used to efficiently evaluate the stability of a networked microgrid system. Specifically, (20) and (21) will be used to estimate the eigenvalue distribution at the edge of the reachable set in each subsystem. After obtaining Geršgorin disks in the ith subsystem, the real part of the approximated eigenvalue located rightmost, $\alpha^e_{i,max}$, can be expressed as follows:

$$\alpha^e_{i,max} = max(s_{kk} + r_k(\mathbf{S_{i,P}})), \tag{32}$$

where $max(\cdot)$ means the maximum value, s_{kk} and $r_k(\mathbf{S_{i,P}})$ can be found in (20). $\alpha^e_{i,max}$ is then used to evaluate the stability of the ith subsystem.

5.3. Stability margin evaluation

Based on the aforementioned reachable set calculation and Geršgorin disks computation, stability margin of an interconnected system under disturbances can be explored as follows:

- If the stability criterion given in (33) is satisfied, it implies the ith subsystem is stable; otherwise, it may not be stable. If this stability criterion holds true in all subsystems, the overall system is stable; otherwise, it might not be stable.

$$\alpha^e_{i,max} \leqslant \alpha_0 \tag{33}$$

  where α_0 is the given threshold.
- If DQG shows the ith subsystem may not be stable, exact eigenvalues will be calculated to further assess its stability. Specifically, the real part of the maximum eigenvalue, i.e., $\alpha_{i,max}$, will be calculated. If the stability criterion given in (34) is satisfied, the ith subsystem is stable; otherwise it is not stable.

$$\alpha_{i,max} \leqslant \alpha_0 \tag{34}$$

- If DQG shows the overall system is stable, disturbances will be enlarged in order to get the stability margin. After setting new disturbances, reachable sets and Geršgorin disks will be calculated correspondingly to evaluate the stability again.

The evaluation process will be terminated when the simulation time ends or the system is always unstable after a given simulation steps. If one of these criteria is satisfied, then stop; otherwise continue power flow calculation and reachable set computation. After stability margin is obtained, predictive control or dispatch [40] can be performed in

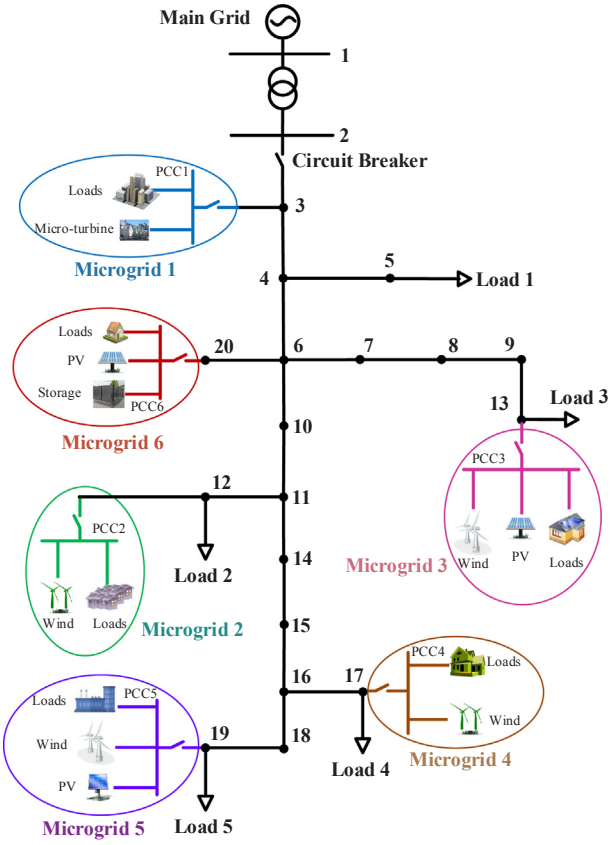

Fig. 4. A typical networked microgrid system.

advance to improve systems' performance. Then an interconnected microgrid system can serve as a resiliency source to better stabilize, restore, or support the main grid.

6. Test and validation

A typical networked microgrid system shown in Fig. 4 is used to test and validate the DQG-based DFA approach by analyzing the impact of DERs on system stability. The circuit breaker is open to form a power island, in order to better illustrate the DER impact. More details of the test system can be found in [28]. The DFA and DQG algorithms are developed on the basis of multiple functions in the CORA toolbox [41]. The simulation step size is set to 0.010 s.

6.1. Verification of microgrid-oriented decomposition

In this test, the original networked microgrids shown in Fig. 4 is partitioned into two subsystems to validate the concept of microgrid-oriented decomposition. Table 1 summarizes the elements of each subsystem.

Based on the aforementioned system partitioning, power flow is calculated in subsystem 1 and subsystem 2 in parallel, which is the inner iteration. Specifically, the corresponding $\mathbf{S}_{1,2}$ ($\mathbf{S}_{i,j}$ given in (26)) in subsystem 1 is the power output from node 6 to node 10; $\mathbf{S}_{2,1}$ in subsystem 2 is the power output from node 10 to node 6. The Newton iteration method is adopted to solve power flow in each subsystem [42]. Subsequentially, an outer iteration is conducted to exchange and update data on the interface of subsystems. The stopping criteria of inner Newton iterations in subsystem 1 and subsystem 2 are set as $1.0e{-}5$, whereas that of Newton iterations on their interface, i.e., the outer iteration, is set as $1.0e{-}3$. In order to better illustrate the changes of values during iterations, the following conversion based on l_2-norm is adopted [43]:

$$\|c_i\|_2 = -10/ln(\|r_i\|_2), \tag{35}$$

where $\|r_i\|_2$ is the l_2-norm of the real value during iterations, $\|c_i\|_2$ is the corresponding converted value.

Fig. 5(a) shows the voltage comparisons between the presented microgrid-oriented decomposition method and the traditional centralized solution, and Fig. 5(b) demonstrates the $l2$-norm changes of variables on the interface in the outer iterations. Fig. 6(a) and (b) illustrates the changes of variables during inner iterations in subsystem 1 and subsystem 2, respectively. From Figs. 5 and 6, it can be seen that:

- Comparisons shown in Fig. 5(a) have verified the feasibility and effectiveness of microgrid-oriented decomposition in networked microgrids.
- The outer iteration process is monotonically decreasing until it is converged, which means the microgrid-oriented decomposition is effective in decoupling and analyzing networked microgrids. Based on the aforementioned stopping criteria of Newton iterations, five outer iterations are needs to obtain the final power flow results. This iteration number depends on the system size and stopping criteria.
- The inner iteration process in each subsystem shows a zigzag decrease. The reason is that calculations in each subsystem are carried out based on the interface data at the previous iteration step, e.g., $\mathbf{S}_{1,2}$ in subsystem 1 and $\mathbf{S}_{2,1}$ in subsystem 2. Even subsystems are converged at the previous iteration, the increments involved in the Newton iteration may become large again after subsystems exchange data between each other.
- Inner iterations in subsystems may be different from each other. For instance, three inner iterations are involved in subsystem 1 within the second outer iteration; whereas only two inner iterations are involved in subsystem 2.

6.2. DFA computation and verification

6.2.1. Reachable set calculation

In this test, multiple active power fluctuations of the PV in Microgrid 5 are investigated to evaluate their impacts on system performance. Specifically, disturbances of ± 1%, ±5%, ±10% and ± 15% are introduced around the PV's baseline power output. Fig. 7 shows the three dimensional reachable sets between the control signals of active power, X_{pi}, and that of reactive power, X_{qi}. Figs. 8 and 9 show the corresponding cross sectional views of the reachable set changes along the time line. To better illustrate the changes of reachable sets, deviation percentages of X_{pi} and X_{qi} around their zonotope centers are provided in Figs. 8 and 9, respectively. More details of X_{pi} and X_{qi} can be found in [28]. From Figs. 7–9, it can be seen that:

- DFA is able to calculate the possible operation boundaries of a networked microgrid system under different uncertainty levels. It validates the presented microgrid-oriented decomposition can be

Table 1
Elements of each subsystem.

Subsystems	Microgrids	Branches
1	1, 3, 6	3–4, 4–5, 4–6, 6–7, 7–8, 8–9, 9–13, 6–20
2	2, 4, 5	10–11, 11–12, 11–14, 14–15, 15–16, 16–17, 16–18, 18–19

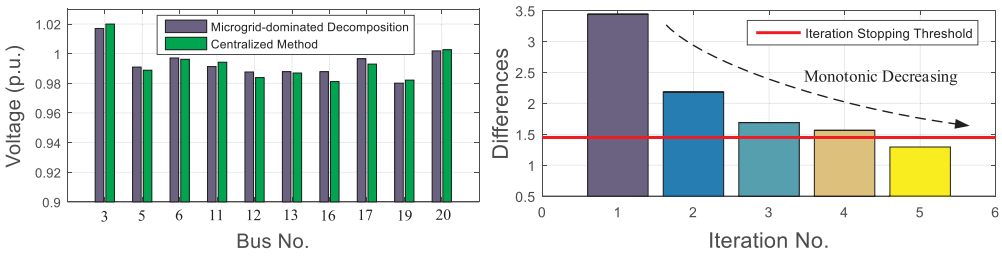

(a) Voltage comparison (b) Voltage differences between iterations

Fig. 5. Voltage results using microgrid-oriented decomposition.

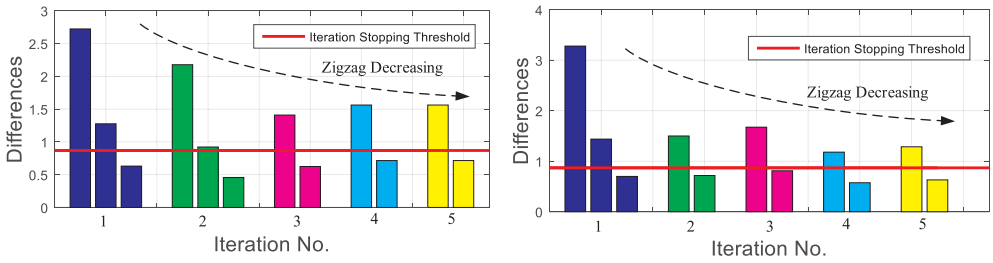

(a) Voltage changes between iterations in the subsystem 1 (b) Voltage changes between iterations in the subsystem 2

Fig. 6. Voltage iterations in subsystem 1 and subsystem 2.

effectively used to solve reachable sets in parallel.

- The sizes of zonotopes increase as the uncertainty level increases. The correctness of DFA result can be further verified by the comparison between DFA and the centralized calculation as shown in [28].
- The comparison between (a) and (b) in Figs. 8 and 9 shows that the disturbances in Microgrid 5 have more impact on the dynamics of Microgrid 5 and Microgrid 4 than that on Microgrid 3 and Microgrid 6 in subsystem 1. The reason is that Microgrid 5 and Microgrid 4 both belong to subsystem 2 and are electrically closer to each other. Detailed comparisons of deviation are given in Table 2.

6.2.2. DFA verification via time domain simulation

Simulations in time domain are used to validate the coverage ability of DFA. For clear and better illustration, seventeen simulation trajectories are selected to compare against the DFA results. Fig. 10 shows the simulation results of X_{pi} and X_{qi} in subsystem 2. It can be observed that:

- The reachable sets are able to fully enclose the time domain trajectories, which validates the over-approximation capability of DFA.
- The over-approximation of reachable sets in this test case is acceptable; however, when the system size highly increases, techniques to reduce the conservativeness may become necessary, e.g., set splitting [44], optimality-based bounds tightening [45].

The observations also show that DFA can obtain the same results as from the centralized formal analysis [28].

6.3. Stability margin analysis via DQG-enabled DFA

In this test, the feasibility of DQG-enabled DFA is demonstrated via calculating the stability margins at different time points. Fig. 11(a) shows the stability margin of Microgrid 5 at 0.2 s; whereas Fig. 11(b)–(d) illustrates the corresponding Geršgorin disks at different operation points, respectively. It can be seen that:

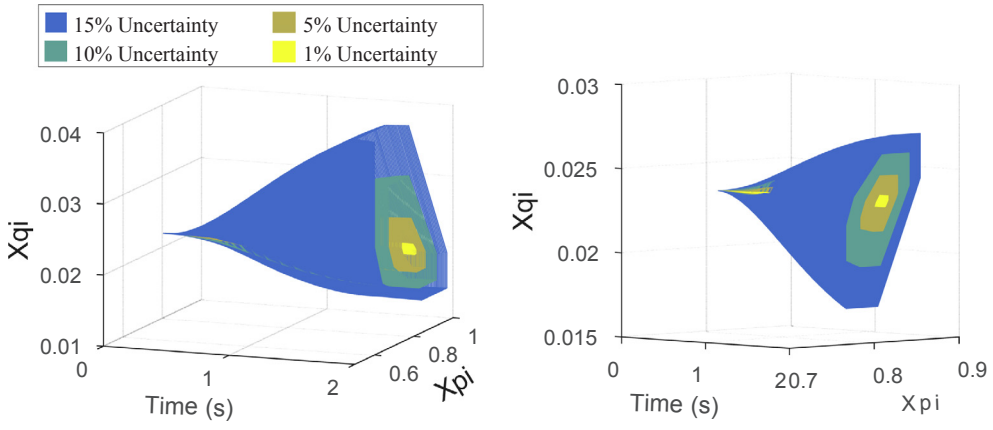

(a) Reachable sets of PV's control signals in Microgrid 5 (b) Reachable sets of wind's control signals in Microgrid 4

Fig. 7. 3-D reachable set of subsystem 2.

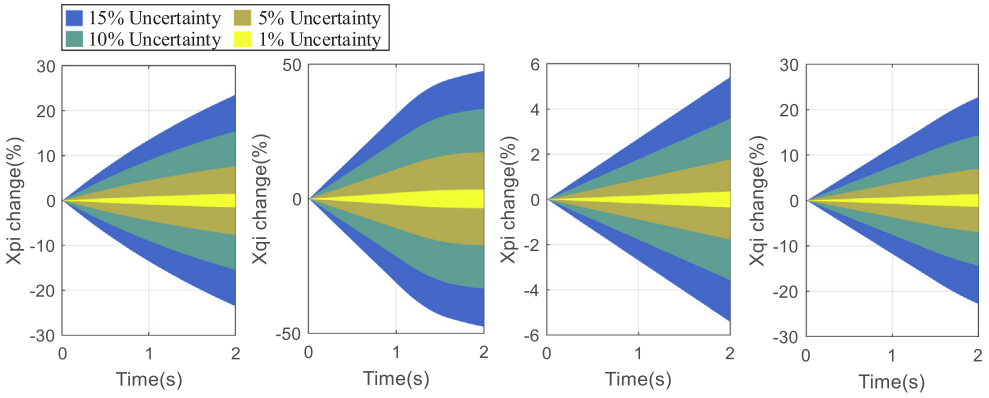

(a) Reachable sets of PV unit's control signals in Microgrid 5

(b) Reachable sets of wind unit's control signals in Microgrid 4

Fig. 8. Reachable sets of subsystem 2 projected to the time line.

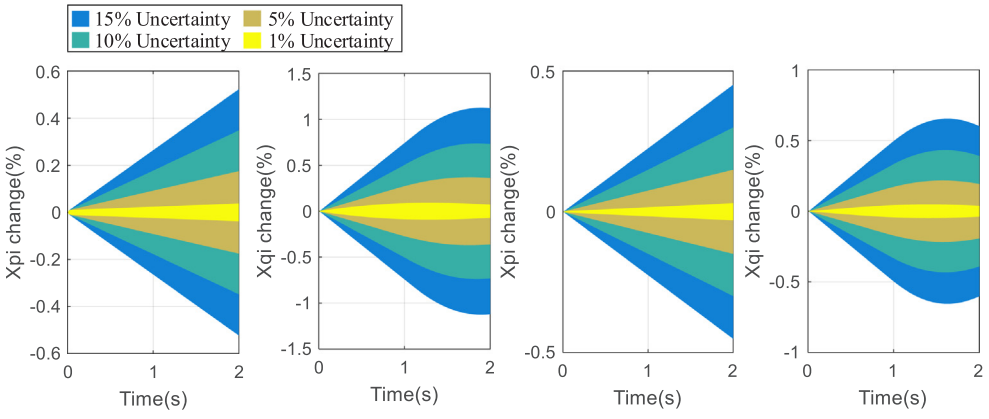

(a) Reachable sets of wind's control signals in Microgrid 3

(b) Reachable sets of storage's control signals in Microgrid 6

Fig. 9. Reachable sets of subsystem 1 projected to the time line.

Table 2
Deviation comparisons of X_{pi} and X_{qi} at 2.0 s.

Subsystems	Microgrids	Deviations	Uncertainties			
			± 1%	± 5%	± 10%	± 15%
Subsystem 1	Microgrid 5	X_{pi}	± 1.53%	± 7.65%	± 15.44%	± 23.52%
		X_{qi}	± 3.49%	± 17.28%	± 33.40%	± 47.56%
	Microgrid 4	X_{pi}	± 0.35%	± 1.77%	± 3.57%	± 5.42%
		X_{qi}	± 1.37%	± 6.94%	± 14.35%	± 22.78%
Subsystem 2	Microgrid 3	X_{pi}	± 0.04%	± 0.18%	± 0.35%	± 0.52%
		X_{qi}	± 0.07%	± 0.36%	± 0.73%	± 1.12%
	Microgrid 6	X_{pi}	± 0.03%	± 0.15%	± 0.30%	± 0.45%
		X_{qi}	± 0.04%	± 0.19%	± 0.39%	± 0.60%

- The stability margin can be efficiently obtained, which validates the feasibility of the DQG-enabled DFA.
- DQG is able to effectively assess the stability when the system operation point is far away from its stability margin, e.g., the point A in Fig. 11(a) and its results in (b). Therefore, in this case, exact eigenvalue calculation is no longer necessary.
- As the uncertainty increases, Geršgorin disks are approaching the y-axis, e.g., the point B in Fig. 11(a) and its results in (c).
- When the system is approaching its stability margin, results from DQG may be conservative (e.g., the point C in Fig. 11(a) and its results in (d)), and thus, exact eigenvalue inspection becomes necessary.

7. Conclusions

Distributed formal analysis, DFA, is presented in this paper to efficiently assess the stability of networked microgrids under heterogeneous disturbances. Distributed quasi-diagonalized Geršgorin, DQG,

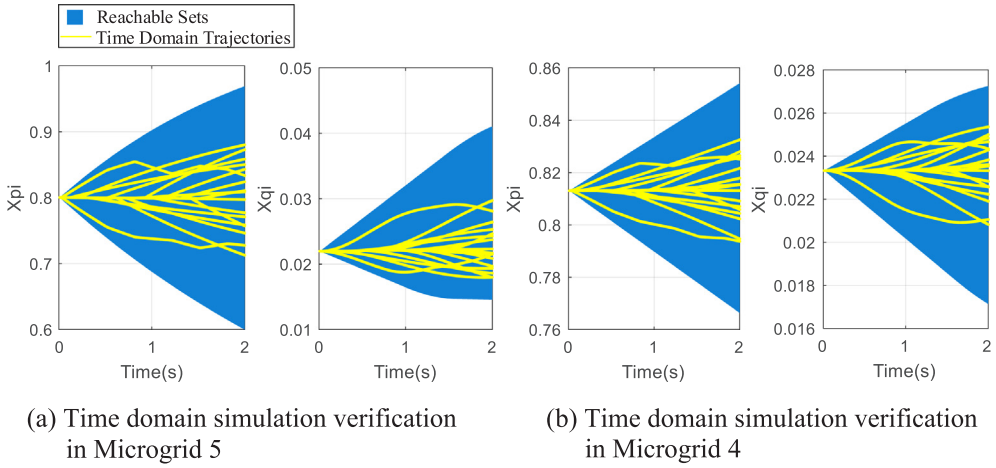

Fig. 10. Time domain simulation verification in subsystem 2.

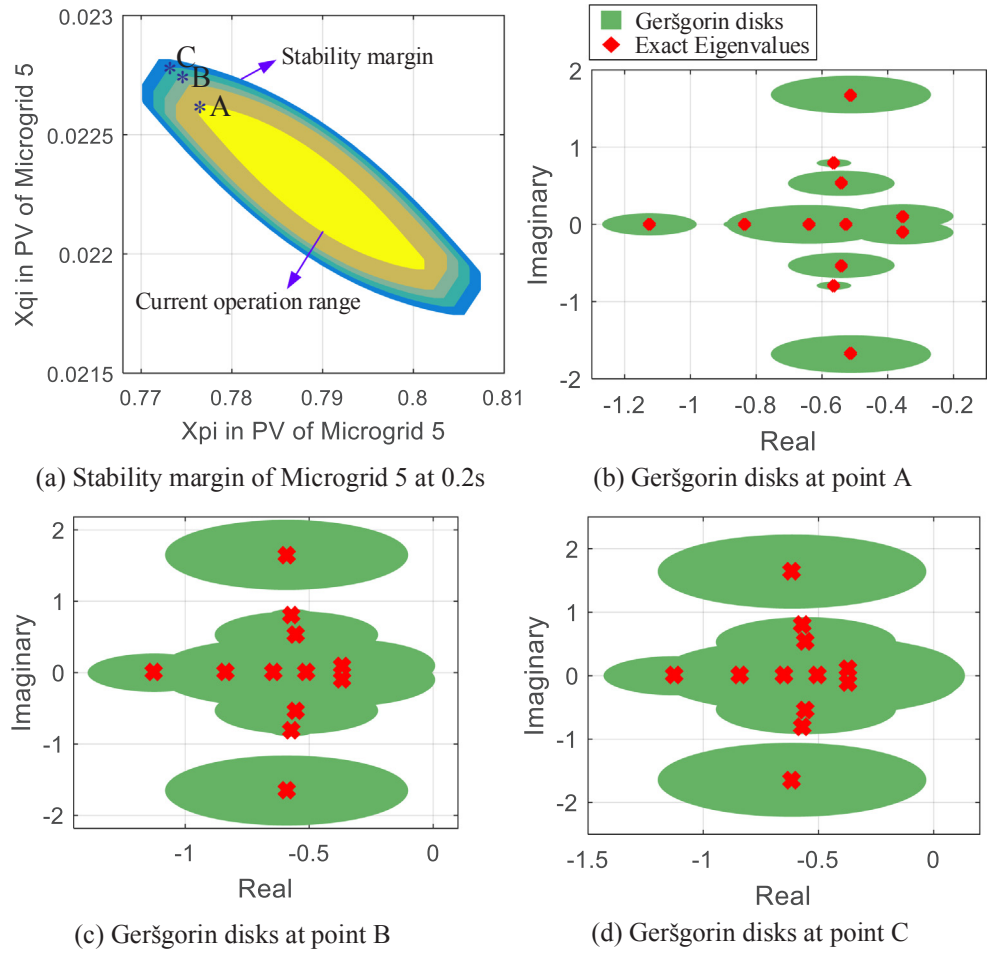

Fig. 11. Stability margin of microgrid 6 at 0.5 s.

is then established to estimate the stability margin of the networked microgrids. A microgrid-oriented decomposition approach is also developed to decouple systems and enable reachable set calculations in parallel. Numerical tests are performed on a typical networked microgrid system. Analyses and tests have confirmed the feasibility and effectiveness of DFA and DQG in the stability analysis of networked microgrids. In the future, DFA and DQG can be further evaluated on a real time simulation test bed or even a real life networked microgrid system. DFA and DQG can be integrated into Advanced Distribution Management System (ADMS) to enable efficient stability assessment and stability margin identification and to provide provably safe and secure operation schemes for networked microgrids. The tools can also be used for planning and designing networked microgrids with guaranteed stability and performance.

Acknowledgment

This material is based upon work supported by the National Science

Foundation, USA under Grant Nos. 1647209 and 1611095, by the Department of Energys Advanced Grid Modeling Program, by funding from the Office of the Provost, University of Connecticut, and by United Technologies Fellowship.

The authors would like to thank Matthias Althoff at Technische Universität München, Germany, for helpful discussions. The authors also would like to thank the anonymous reviewers for the valuable comments.

References

[1] Wang Z, Chen B, Wang J, Begovic MM, Chen C. Coordinated energy management of networked microgrids in distribution systems. IEEE Trans Smart Grid 2015;6(1):45–53.
[2] Kou P, Liang D, Gao L. Distributed EMPC of multiple microgrids for coordinated stochastic energy management. Appl Energy 2017;185:939–52.
[3] Lv T, Ai Q. Interactive energy management of networked microgrids-based active distribution system considering large-scale integration of renewable energy resources. Appl Energy 2016;163:408–22.
[4] Ren L, Qin Y, Li Y, Zhang P, Wang B, Luh PB, Han S, Orekan T, Gong T, et al. Enabling resilient distributed power sharing in networked microgrids through software defined networking. Appl Energy 2018;210:1251–65.
[5] He J, Li Y, Wang C, Pan Y, Zhang C, Xing X. Hybrid microgrid with parallel-and series-connected microconverters. IEEE Trans Power Electron 2018;33(6):4817–31.
[6] Haddadian H, Noroozian R. Multi-microgrids approach for design and operation of future distribution networks based on novel technical indices. Appl Energy 2017;185:650–63.
[7] Wang C, Wu J, Ekanayake J, Jenkins N. Smart electricity distribution networks. CRC Press; 2017.
[8] Fang X, Yang Q, Wang J, Yan W. Coordinated dispatch in multiple cooperative autonomous islanded microgrids. Appl Energy 2016;162:40–8.
[9] Li P, Ji H, Wang C, Zhao J, Song G, Ding F, et al. Optimal operation of soft open points in active distribution networks under three-phase unbalanced conditions. IEEE Trans Smart Grid 2017:1–12. http://dx.doi.org/10.1109/TSG.2017.2739999.
[10] Bie Z, Zhang P, Li G, Hua B, Meehan M, Wang X. Reliability evaluation of active distribution systems including microgrids. IEEE Trans Power Syst 2012;27(4):2342–50.
[11] Li X, Guo L, Li Y, Guo Z, Hong C, Zhang Y, et al. A unified control for the dc-ac interlinking converters in hybrid ac/dc microgrids. IEEE Trans Smart Grid 2017:1–13. http://dx.doi.org/10.1109/TSG.2017.2715371.
[12] Li Y, Zhang P, Ren L, Orekan T. A Geršgorin theory for robust microgrid stability analysis. In: PES general meeting; 2016. p. 1–5.
[13] Li Y, Zhang P, Li W, Debs JN, Ferrante DA, Kane DJ, et al. Non-detection zone analytics for unintentional islanding in distribution grid integrated with distributed energy resources. IEEE Trans Sustain Energy 2018:1–10. http://dx.doi.org/10.1109/TSTE.2018.2830748.
[14] Li Y, Gao W, Jiang J. Stability analysis of microgrids with multiple der units and variable loads based on MPT. In: PES general meeting conference and exposition, 2014 IEEE. IEEE; 2014. p. 1–5.
[15] Nikmehr N, Najafi-Ravadanegh S, Khodaei A. Probabilistic optimal scheduling of networked microgrids considering time-based demand response programs under uncertainty. Appl Energy 2017;198:267–79.
[16] Wang C, Fu X, Li P, Wu J, Wang L. Multiscale simulation of power system transients based on the matrix exponential function. IEEE Trans Power Syst 2017;32(3):1913–26.
[17] Duan N, Sun K. Power system simulation using the multistage adomian decomposition method. IEEE Trans Power Syst 2017;32(1):430–41.
[18] Kwon J, Wang X, Blaabjerg F, Bak CL. Frequency-domain modeling and simulation of dc power electronic systems using harmonic state space method. IEEE Trans Power Electron 2017;32(2):1044–55.
[19] Chang H-D, Chu C-C, Cauley G. Direct stability analysis of electric power systems using energy functions: theory, applications, and perspective. Proc IEEE 1995;83(11):1497–529.
[20] Canizares C, Fernandes T, Geraldi E, Gerin-Lajoie L, Gibbard M, Hiskens I, et al. Benchmark models for the analysis and control of small-signal oscillatory dynamics in power systems. IEEE Trans Power Syst 2017;32(1):715–22.
[21] Chiang H-D, Wu FF, Varaiya PP. A bcu method for direct analysis of power system transient stability. IEEE Trans Power Syst 1994;9(3):1194–208.
[22] Chiang H-D, Wu F, Varaiya P. Foundations of direct methods for power system transient stability analysis. IEEE Trans Circ Syst 1987;34(2):160–73.
[23] Ghahremani E, Kamwa I. Local and wide-area PMU-based decentralized dynamic state estimation in multi-machine power systems. IEEE Trans Power Syst 2016;31(1):547–62.
[24] Salinas SA, Li P. Privacy-preserving energy theft detection in microgrids: a state estimation approach. IEEE Trans Power Syst 2016;31(2):883–94.
[25] Sánchez-García RJ, Fennelly M, Norris S, Wright N, Niblo G, Brodzki J, et al. Hierarchical spectral clustering of power grids. IEEE Trans Power Syst 2014;29(5):2229–37.
[26] Zhang P, Marti J, Dommel H. Network partitioning for real-time power system simulation. In: International conference on power system transients. Montreal (Canada); 2005.
[27] Crow M, Ilic M. The parallel implementation of the waveform relaxation method for transient stability simulations. IEEE Trans Power Syst 1990;5(3):922–32.
[28] Li Y, Zhang P, Luh PB. Formal analysis of networked microgrids dynamics. IEEE Trans Power Syst 2018;33(3):3418–27.
[29] Li Y, Zhang P. Reachable set calculation and analysis of microgrids with power-electronic-interfaced renewables and loads. In: Power and energy society general meeting, 2018 IEEE. IEEE; 2018. p. 1–5.
[30] Althoff M. Formal and compositional analysis of power systems using reachable sets. IEEE Trans Power Syst 2014;29(5):2270–80.
[31] El-Guindy A, Chen YC, Althoff M. Compositional transient stability analysis of power systems via the computation of reachable sets. In: American control conference (ACC), 2017. IEEE; 2017. p. 2536–43.
[32] Iqbal M, Leth J, Ngo TD. Cartesian product-based hierarchical scheme for multi-agent systems. Automatica 2018;88:70–5.
[33] Wang C, Li Y, Peng K, Hong B, Wu Z, Sun C. Coordinated optimal design of inverter controllers in a micro-grid with multiple distributed generation units. IEEE Trans Power Syst 2013;28(3):2679–87.
[34] Althoff M, Krogh BH. Zonotope bundles for the efficient computation of reachable sets. in: 50th IEEE conference on decision and control and European control conference (CDC-ECC), 2011. IEEE; 2011. p. 6814–21.
[35] Friedenberg N, Oneto A, Williams RL. Minkowski sums and hadamard products of algebraic varieties. Combinatorial algebraic geometry. Springer; 2017. p. 133–57.
[36] Li Y, Zhang P, Zhang L, Wang B. Active synchronous detection of deception attacks in microgrid control systems. IEEE Trans Smart Grid 2017;8(1):373–5.
[37] Xie L, Baytas IM, Lin K, Zhou J. Privacy-preserving distributed multi-task learning with asynchronous updates. In: Proceedings of the 23rd ACM SIGKDD international conference on knowledge discovery and data mining. ACM; 2017. p. 1195–204.
[38] Althoff M, Krogh BH. Reachability analysis of nonlinear differential-algebraic systems. IEEE Trans Autom Control 2014;59(2):371–83.
[39] Wang D, Wu X, Pan L, Shen J, Lee K. A novel zonotope-based set-membership identification approach for uncertain system. In: 2017 IEEE conference on control technology and applications (CCTA). IEEE; 2017. p. 1420–5.
[40] Vazquez S, Rodriguez J, Rivera M, Franquelo LG, Norambuena M. Model predictive control for power converters and drives: advances and trends. IEEE Trans Indust Electron 2017;64(2):935–47.
[41] Althoff M. CORA 2016 manual.
[42] Conejo AJ, Baringo L. Power flow. Power system operations. Springer; 2018. p. 97–135.
[43] Robert C. Machine learning, a probabilistic perspective; 2014.
[44] Althoff M, Stursberg O, Buss M. Reachability analysis of nonlinear systems with uncertain parameters using conservative linearization. In: 47th IEEE conference on decision and control, 2008, CDC 2008. IEEE; 2008. p. 4042–8.
[45] Araya I, Reyes V. Interval branch-and-bound algorithms for optimization and constraint satisfaction: a survey and prospects. J Glob Optim 2016;65(4):837–66.